Separation Science and Technology
Publication details, including instructions for authors and subscription information:
http://www.informaworld.com/smpp/title~content=t713708471

Unsteady-State Permeate Flux of Crossflow Microfiltration

Dong-Jang Chang[a]; Shyh-Jye Hwang[a]
[a] DEPARTMENT OF CHEMICAL ENGINEERING, NATIONAL TSING HUA UNIVERSITY HSINCHU, TAIWAN, REPUBLIC OF CHINA

To cite this Article Chang, Dong-Jang and Hwang, Shyh-Jye(1994) 'Unsteady-State Permeate Flux of Crossflow Microfiltration', Separation Science and Technology, 29: 12, 1593 — 1608
To link to this Article: DOI: 10.1080/01496399408007376
URL: http://dx.doi.org/10.1080/01496399408007376

SEPARATION SCIENCE AND TECHNOLOGY, **29**(12), pp. 1593–1608, 1994

Unsteady-State Permeate Flux of Crossflow Microfiltration

DONG-JANG CHANG and SHYH-JYE HWANG*
DEPARTMENT OF CHEMICAL ENGINEERING
NATIONAL TSING HUA UNIVERSITY
HSINCHU, TAIWAN 30043, REPUBLIC OF CHINA

ABSTRACT

In this study a membrane filtration cell was installed to investigate the variation of permeate flux with filtration time under various operating conditions including crossflow velocity, pressure drop, particle concentration, membrane pore size, particle size, pH, and electrolyte concentration. The dimensions of the filtration channel in the CFMF cell were 6 cm × 0.6 cm × 0.036 cm, and the flow of the suspension in the channel was controlled under the laminar flow region. Spherical polystyrene latex particles of 0.303, 0.606, and 1.020 μm were used as the suspension particles in the experiments. The density of the particles was 1.05 g/cm^3. It was found that the unsteady-state permeate flux increased with an increase in particle size, membrane pore size, or crossflow velocity, but decreased with an increase in particle concentration or electrolyte concentration in the suspension. A mathematical model based on mass balance and hydrodynamic theory was developed in this study. In addition, the effect of cake growth and particle concentration decline during experiments on the permeate flux were also considered in this model. This model predicts satisfactorily the unsteady-state permeate flux of CFMF under various operating conditions.

INTRODUCTION

The crossflow microfiltration (CFMF) technique, which can remove particles of 0.1–10 μm effectively, has been widely developed and utilized in water and wastewater treatment processes. The major factor affecting the separation efficiency of CFMF is the formation of a cake layer on the

* To whom correspondence should be addressed.

surface of the membrane. The permeate flux decreases with filtration time due to increasing hydraulic resistance of the growing cake layer. However, for every operating condition, a steady state will be reached where the cake thickness and permeate flux remain constant. This is in contrast to the conventional filtration process in which the cake keeps growing with filtration time.

Several hydrodynamic models have been developed to describe the performance of CFMF under steady-state conditions (1–5). However, hydrodynamic models predicting the unsteady-state permeate flux of CFMF are limited (6–9). Moreover, the applicability of these mathematical models over a wide range of operating conditions including crossflow velocity, pressure drop, particle concentration, membrane pore size, particle size, pH, and electrolyte concentration is questionable because all of the coefficients appearing in those models are obtained from empirical correlations. Since these operating parameters greatly affect the performance of CFMF in water and wastewater treatment processes, a more universal model describing the behavior of CFMF under various operating conditions is urgently needed. Thus, a mathematical model based on mass balance and hydrodynamic theory is proposed in this study to predict the unsteady-state permeate flux of CFMF under various operating conditions.

THEORETICAL DEVELOPMENT

Hydrodynamic Model

Three assumptions were made in the development of the model:

1. Particles cannot penetrate into or through the membrane.
2. Uniform voidage of the cake during the cake growth period.
3. Particles deposited beneath the membrane to form the cake during unsteady state will not be resuspended.

A schematic representation of model is shown in Fig. 1. As shown, deposition of particles below the membrane takes place due to the drag force resulting from convective transport of the permeate flux, u_p. The permeate flux is evaluated by Darcy's equation for constant pressure filtration:

$$u_p = \frac{\Delta P}{\mu(R_m + R_c)} \tag{1}$$

However, there is backtransport of particles away from the vicinity of the cake due to backtransport velocity, u_t. The backtransport velocity is the summation of velocities due to lateral migration, shear-induced diffusion, Brownian diffusion, gravity, and double-layer repulsion. The lateral

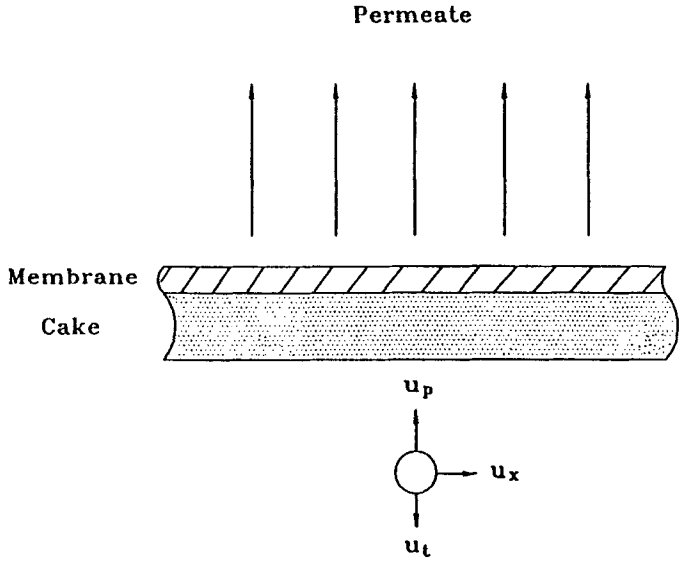

FIG. 1 Schematic representation of the model.

lift velocity, u_l, was proposed by Altena and Belfort (10):

$$u_l = \frac{0.43\rho u_o^2 d_p^3}{\mu h^2} \tag{2}$$

The values of the velocities due to shear-induced diffusion (u_s), Brownian diffusion (u_b), and double-layer repulsion (u_e) were obtained by Cohen and Probstein (11) and Wiesner et al. (12):

$$u_s = \frac{u_o d_p^2}{20h^2} \tag{3}$$

$$u_b = \frac{2KT}{3\pi\mu d_p h} \tag{4}$$

$$u_e = \frac{1}{\mu}\left(\frac{2\epsilon_o \zeta^2}{45\pi X_d} - \frac{A}{36\pi X_d^2}\right) \tag{5}$$

The velocity due to gravity, u_g, can be calculated by the equation proposed by Hartman et al. (13). However, u_g in this study is much smaller than the other velocities. Thus, it is negligible.

Therefore, the cake resistance, R_c, in Eq. (1) can be obtained as follows:

$$R_c = \rho_p \alpha C \int (u_p - u_l - u_s - u_b - u_e)\, dt \tag{6}$$

Equation (1) can then be rearranged as

$$u_p = \frac{\Delta P}{\mu[R_m + \rho_p \alpha C \int (u_p - u_l - u_s - u_b - u_e)\, dt]} \tag{7}$$

Integration of Eq. (7) gives

$$\int u_p\, dt = u_t t + \frac{\Delta P}{\rho_p \mu \alpha C u_p} - \frac{R_m}{\rho_p \alpha C} \tag{8}$$

where $u_t = u_l + u_s + u_b + u_e$.

During each experiment the volumetric flow rate of the suspension was kept constant, but the effective channel height of the filtration module decreased due to the growth of the cake under the surface of the membrane. Thus, the crossflow velocity must be modified as

$$u_{oi} = \left[u_o + \frac{(u_{po} - u_{pi})A_m}{A_b}\right] \frac{h}{h - h_{ci}} \tag{9}$$

where u_o is the crossflow velocity of the suspension measured at the outlet of the filtration cell, and h_{ci} is defined by

$$h_{ci} = \frac{\Delta P - \mu u_{pi} R_m}{\mu u_{pi}} \times \frac{d_p^2 \epsilon_c^3}{180(1 - \epsilon_c)^2} \tag{10}$$

In addition, the velocities due to lateral migration, shear-induced diffusion, and Brownian diffusion should be modified as

$$u_{li} = \frac{0.43 \rho u_{oi}^2 d_p^3}{\mu(h - h_{ci})^2} \tag{11}$$

$$u_{si} = \frac{u_{oi} d_p^2}{20(h - h_{ci})^2} \tag{12}$$

$$u_{bi} = \frac{2KT}{3\pi \mu d_p (h - h_{ci})} \tag{13}$$

Moreover, the particle concentration in the suspension was also modified:

$$C_i = C - \frac{(1 - \epsilon_c) h_{ci} A_m}{V_t} \tag{14}$$

A stepwise iterative procedure was then used to calculate the unsteady permeate flux from Eqs. (8) and (11)–(14).

EXPERIMENTAL APPARATUS AND METHODS

The schematic diagram of the experimental setup is shown in Fig. 2. The suspension of spherical polystyrene latex particles was delivered from

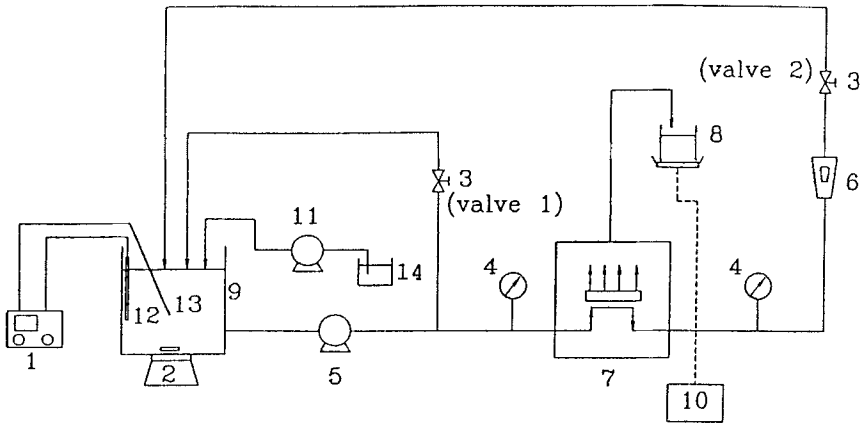

1. temp controller	2. stirrer
3. valves	4. pressure gauge
5. squeezing pump	6. rotameter
7. filtration cell	8. electronic balance
9. stock tank	10. recorder
11. micro-metering pump	12. heater
13. temp sensor	14. deionized water beaker

FIG. 2 Schematic diagram of experimental setup.

a stock tank equipped with a temperature controller to a CFMF cell by a squeezing pump. The diameters and density of the polystyrene latex particles were 0.303, 0.606, and 1.020 μm, and 1.05 g/cm^3, respectively. The dimensions of the filtration channel in the CFMF cell were 6 cm × 0.6 cm × 0.036 cm, and the filters used were Durapore membranes made by Millipore. The membrane pore sizes were 0.1, 0.2, 0.45, and 0.65 μm. Note that for all experimental runs the diameter of the suspension particles was always much larger than the membrane pore size in order to prevent particle penetration into or through the membrane.

In all experiments the suspension flowed under the membrane of the CFMF cell, and the flow rate and inlet and outlet pressures of the suspension were measured by a rotameter and pressure gauges, respectively. The suspension flow was always kept in the laminar flow region. The permeate flux through the membrane was measured by an electronic balance and recorded by a recorder. The suspension flowing out of the CFMF

cell was recycled to the stock tank, and deionized water was added to the suspension by a micro-metering pump to keep the total volume of the suspension in the stock tank constant.

The effects of various operating conditions, including crossflow velocity, pressure drop, particle size, electrolyte concentration, pH, particle concentration, and membrane pore size, on the unsteady-state permeate flux were investigated.

RESULTS AND DISCUSSION

Determination of the Specific Resistance (α) and Voidage (ϵ_c) of the Cake

For constant pressure crossflow microfiltration, the relationship among the permeate flux, pressure drop across the membrane, membrane resistance, and cake resistance can be described by Darcy's equation:

$$u_p = \frac{1}{A_m}\frac{dV}{dt} = \frac{\Delta P}{\mu(R_m + R_c)} \tag{15}$$

where

$$R_c = \frac{\alpha C \rho_p V}{A_m} = \frac{\alpha W_c}{A_m} \tag{16}$$

$$W_c = h_{ci}\rho_p A_m(1 - \epsilon_c) \tag{17}$$

By substituting Eq. (16) into Eq. (15) and then integrating Eq. (15), we obtain the well-known filtration equation

$$\frac{t}{V} = \frac{R_m \mu}{\Delta P A_m} + \alpha\left[\frac{\mu\rho_p C}{2\Delta P A_m^2}\right] V \tag{18}$$

Note that V is obtained from dead-end filtration experiments. The specific resistance, α, is obtained from the slope of the linear plot of t/V vs V. The voidage of the cake, ϵ_c, can then be evaluated by the Carman–Kozeny equation:

$$\alpha = \frac{180(1 - \epsilon_c)}{\epsilon_c^3 \rho_p d_p^2} \tag{19}$$

Unsteady-State Permeate Flux

Unsteady-state permeate flux of CFMF under various operating conditions and the accuracy of the mathematical model developed in this study are described as follows.

Effect of Particle Size

The effect of the suspension particle size on the unsteady-state permeate flux of CFMF is shown in Fig. 3. As shown, the permeate flux increases with an increase in particle size. This is due to the fact that the lateral lift velocity and the shear-induced velocity increase as particle size is increased. As a result, cake thickness decreases with increasing particle size. Therefore, a higher permeate flux is obtained for suspensions of larger particle size. Also shown in this figure is that the permeate flux predicted by the mathematical model agrees very well with that obtained experimentally.

Effect of Membrane Pore Size

Membranes with pore size of 0.1, 0.2, 0.45, and 0.65 μm were used to study the effect of membrane pore size on the unsteady-state permeate flux. The results are shown in Fig. 4. Membranes with larger pores have lower membrane resistance, and thus higher permeate fluxes were obtained. In addition, because of higher permeate fluxes, the cakes grow

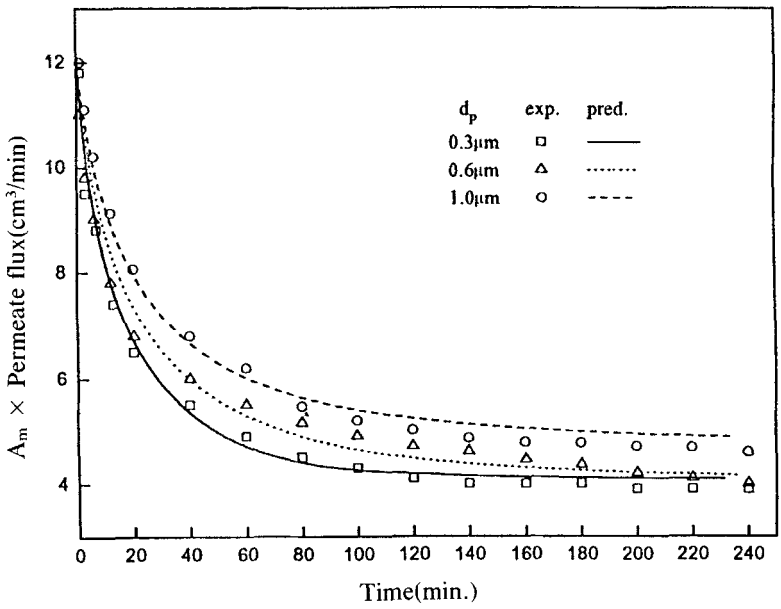

FIG. 3 Effect of particle size on permeate flux (d_m = 0.1 μm, ΔP = 3.8 × 10^4 Nt/m², T = 30°C, pH 6.6, u_o = 1.8 m/s, C = 50 ppmv).

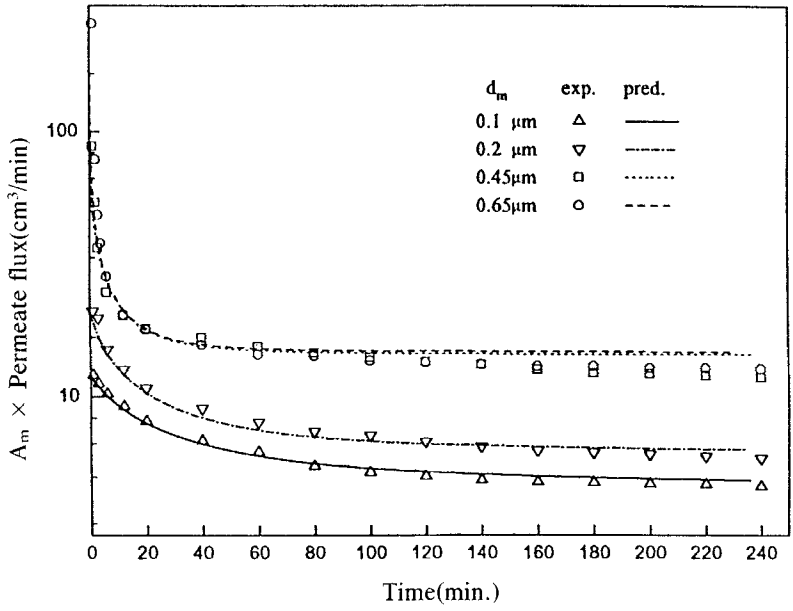

FIG. 4 Effect of pore size on permeate flux (d_p = 1.0 μm, ΔP = 3.8 × 10^4 Nt/m², T = 30°C, pH 6.6, u_o = 1.8 m/s, C = 50 ppmv).

faster for larger pore size membranes. As a result, a sharp drop of permeate flux occurs in the initial filtration period, and a shorter time is needed to reach the steady-state condition. Note in this figure that model predictions are in agreement with experimental results.

Effect of Crossflow Velocity

The effect of crossflow velocity on the permeate flux is shown in Figs. 5A and 5B. As shown in Fig. 5A, the effect of crossflow velocity on the permeate flux is negligible for a particle size of 0.3 μm. On the other hand, as shown in Fig. 5B, the permeate flux increases with increasing crossflow velocity for a particle size of 1.0 μm. These results are similar to those reported by Davis (14) and Wiesner and Chellam (15). This is due to the fact that the backtransport velocity of 0.3 μm particle is dominated by double-layer repulsion and Brownian diffusion, which are not affected by crossflow velocity. However, the backtransport velocity of a 1.0 μm particle is dominated by the lateral lift velocity and the shear-induced velocity, which are affected by crossflow velocity. It should be noted that there is good agreement between model predictions and experiment results.

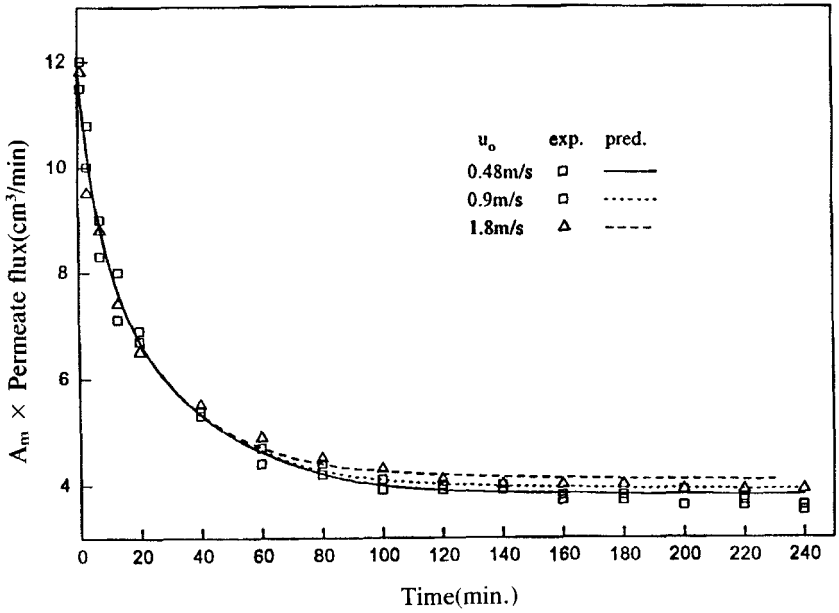

FIG. 5A Effect of crossflow velocity on permeate flux (d_m = 0.1 μm, d_p = 0.3 μm, ΔP = 3.8 × 10^4 Nt/m², T = 30°C, pH 6.6, C = 50 ppmv).

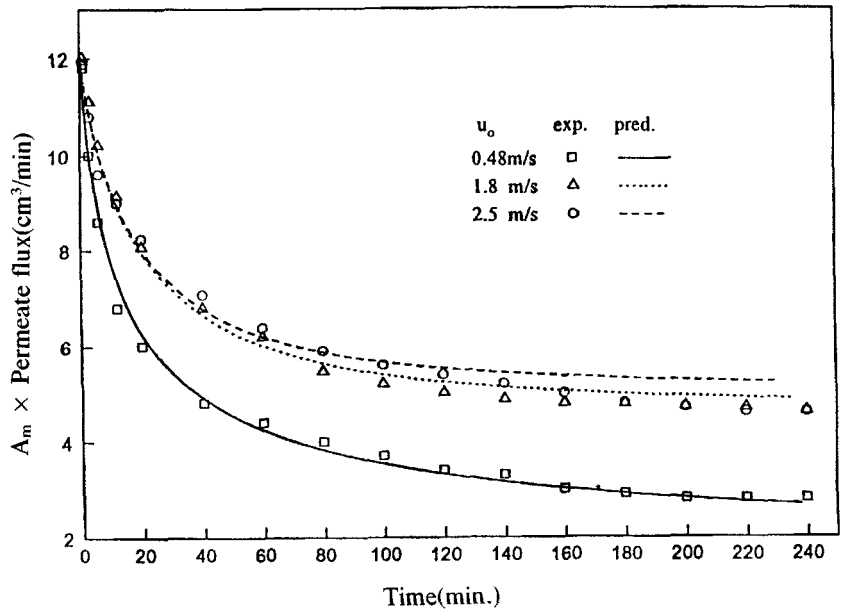

FIG. 5B Effect of crossflow velocity on permeate flux (d_m = 0.1 μm, d_p = 1.0 μm, ΔP = 3.8 × 10^4 Nt/m², T = 30°C, pH 6.6, C = 50 ppmv).

Effect of Pressure Drop

The effect of pressure drop across the membrane on the permeate flux was studied using three different pressure drops: 1.7×10^4, 3.8×10^4, and 5.2×10^4 Nt/m^2. Figure 6 indicates that the permeate flux first increases and then decreases with increasing pressure drop. It is seen from Darcy's equation that the permeate flux increases with pressure drop. However, the voidage of the cake is low at a high pressure drop. As a result, the permeate flux is reduced at a high pressure drop due to high cake resistance. Therefore, a maximum permeate flux exists due to these two counteracting effects.

Effect of Particle Concentration in the Suspension

The effect of particle concentration in the suspension was studied using three different concentrations: 25, 50, and 200 ppmv. The results are shown in Fig. 7. The cake grows faster for a higher particle concentration in the suspension, so there is a sharp drop of permeate flux in the initial filtration period. In addition, the permeate flux decreases with particle

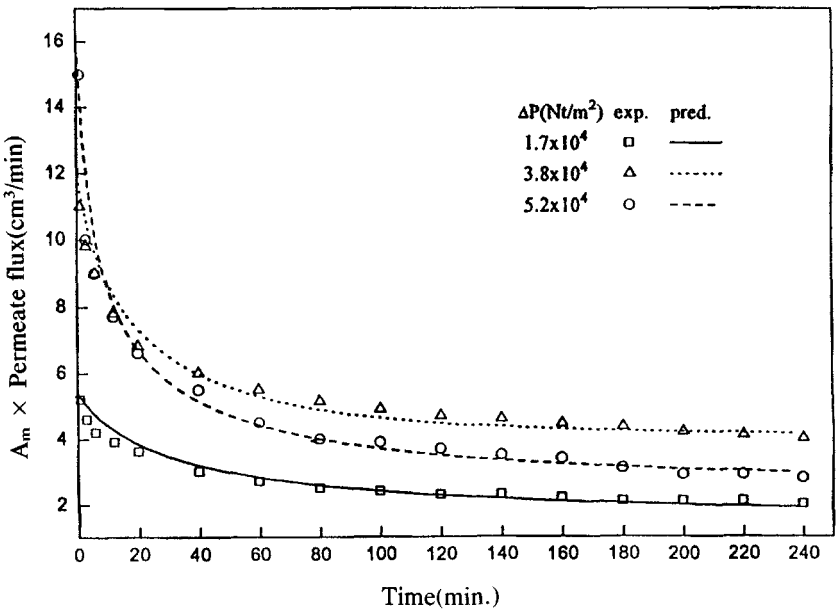

FIG. 6 Effect of pressure drop on permeate flux (d_m = 0.1 μm, d_p = 0.6 μm, T = 30°C, pH 6.6, u_o = 1.8 m/s, C = 50 ppmv).

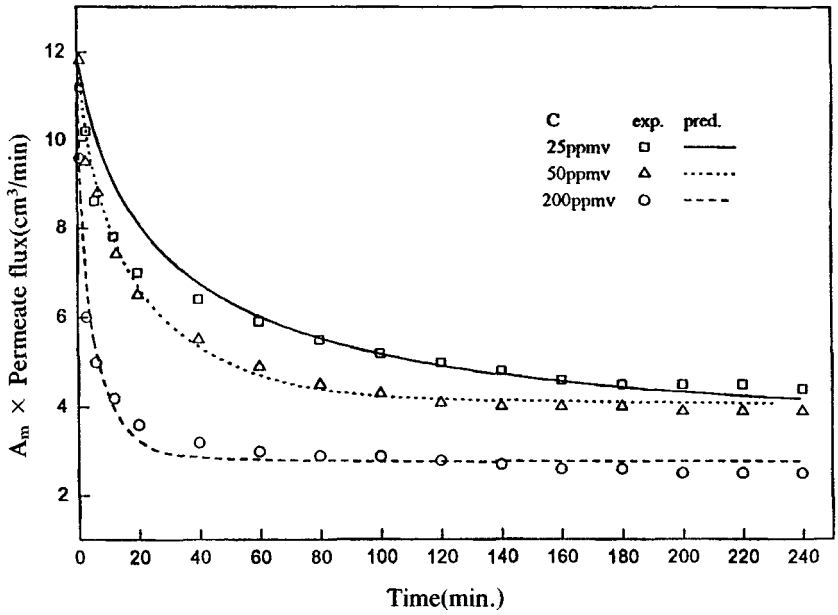

FIG. 7 Effect of particle concentration on permeate flux (d_m = 0.1 μm, d_p = 0.3 μm, ΔP = 3.8 × 10^4 Nt/m², T = 30°C, pH 6.6, u_o = 1.8 m/s).

concentration. Furthermore, good agreement between model predictions and experimental data is shown in this figure.

Effect of Electrolyte Concentration

NaCl solution was used as the electrolyte in the experiments. Figure 8 indicates that the permeate flux decreases as NaCl concentration in the suspension is increased. This is due to the fact that the zeta potential decreases as the electrolyte concentration is increased (Table 1). As a consequence, the double-layer repulsion force between particles and backdiffusion decrease (16, 17), and the cake thickness is larger. Therefore, the unsteady-state permeate flux decreases with increasing NaCl concentration.

Also shown in this figure is that the permeate flux in the initial period predicted by the model is higher than that obtained experimentally. This may be due to the fact that the particles in the suspension are more easily attracted to the membrane because of the opposite charges carried by the particles and the membrane. Thus, in the initial period the cake grows

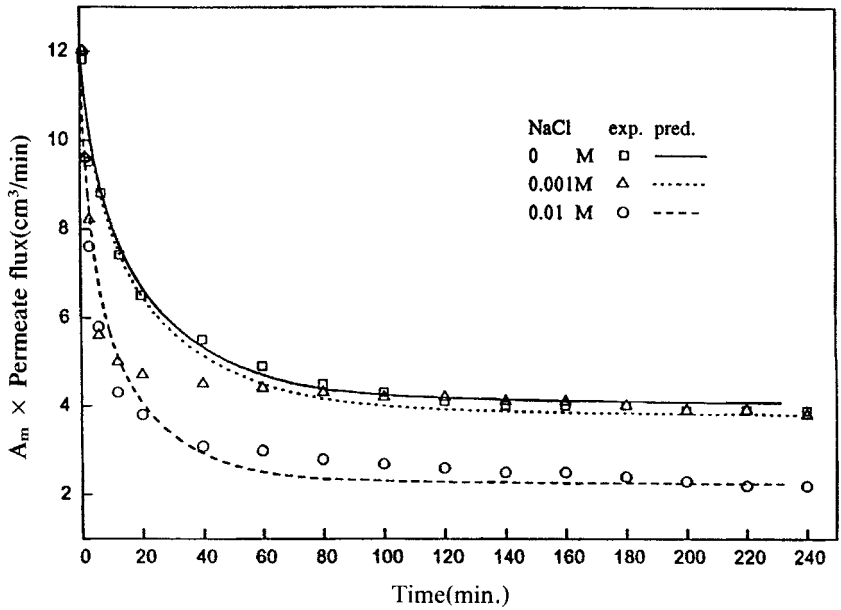

FIG. 8 Effect of electrolyte concentration on permeate flux (d_m = 0.1 μm, d_p = 0.3 μm, ΔP = 3.8 × 10^4 Nt/m², T = 30°C, pH 6.6, u_o = 1.8 m/s, C = 50 ppmv).

faster, and the permeate flux decreases more than is predicted by the model.

Effect of pH

The effect of pH was studied using four different pH values: 3, 4, 6.6, and 9.5. Solutions of 15 M HCl and 15 M NaOH were used to adjust the pH of the suspension, and 1 M NaCl solution was used to keep the ionic strength of the suspension at the same value in all experiments. Figure 9

TABLE 1
Zeta Potential of the Suspension of 0.303 μm Particles at pH 6.6 under Various NaCl Concentrations

NaCl concentration (M)	Zeta potential (mV)
0	−37
0.001	−22
0.01	−17

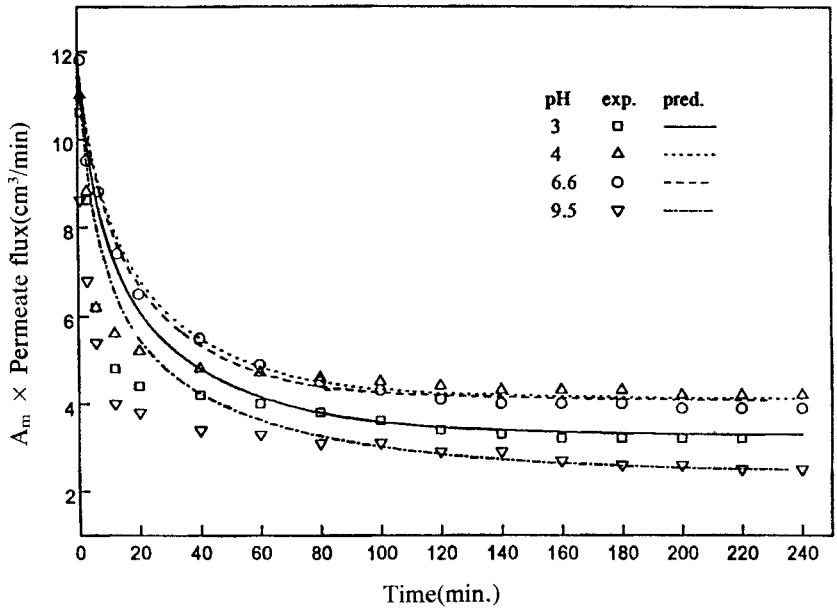

FIG. 9 Effect of pH on permeate flux (d_m = 0.1 μm, d_p = 0.3 μm, ΔP = 3.8 × 10^4 Nt/m^2, T = 30°C, pH 6.6, u_o = 1.8 m/s, C = 50 ppmv).

shows that the permeate flux first increases and then decreases with pH. Note in this figure that the experimental results are lower than the model predictions during the initial period of filtration. This is similar to what is shown in Fig. 8, and the probable reason for this has been mentioned previously, i.e., opposite charges carried by the particles and the membrane.

CONCLUSIONS

Experiments were conducted to study crossflow microfiltration of suspensions of spherical polystyrene latex particles. It was found that the unsteady-state permeate flux increased with increasing particle size, membrane pore size, or crossflow velocity. However, it decreased with increasing particle concentration or electrolyte concentration in the suspension.

Furthermore, the permeate flux first increased and then decreased with pressure drop across the membrane or the pH of the suspension. Thus, an optimum pressure drop or pH exists under which the permeate flux is maximum.

A mathematical model based on mass balance and hydrodynamic theory was developed in this study. This model can accurately predict the unsteady-state permeate flux of crossflow microfiltration under various operating conditions.

NOTATIONS

A	Hamaker constant (J)
A_m	filtration area of membrane (m^2)
A_b	cross section area of channel (m^2)
C	particle concentration in the suspension (ppmv)
C_i	modification of C (ppmv)
d_m	membrane pore size (m)
d_p	particle diameter (m)
h	clearance of crossflow channel (m)
h_c	cake thickness (m)
h_{ci}	modification of h_c (m)
K	Boltzmann constant (J/K)
ΔP	pressure drop across membrane (Nt/m^2)
R_c	cake resistance (1/m)
R_m	membrane resistance (1/m)
T	temperature (K)
t	filtration time (min)
u_b	Brownian diffusion (m/s)
u_{bi}	modification of u_b (m/s)
u_e	velocity due to double-layer repulsion (m/s)
u_g	velocity due to gravity (m/s)
u_l	lateral lift velocity (m/s)
u_{li}	modification of u_l (m/s)
u_o	crossflow velocity (m/s)
u_{oi}	modification of u_o (m/s)
u_p	permeate flux (m/s)
u_{pi}	modification of u_p (m/s)
u_{po}	initial permeate flux (m/s)
u_s	shear-induced velocity (m/s)
u_{si}	modification of u_s (m/s)
u_t	backtransport velocity (m/s)
u_x	axial velocity of particle (m/s)
V	cumulative volume of the permeate (m^3)
V_t	volume of the suspension in stock tank (m^3)
W_c	weight of cake (kg)
X_d	Debye length (m)

Greek Letters

α	specific resistance of cake (m/kg)
μ	viscosity of the suspension (kg/ms)
ϵ_o	dielectric constant of the suspension (Nt/V^2)
ϵ_c	cake voidage
ζ	zeta potential (V)
ρ	water density (kg/m^3)
ρ_p	particle density (kg/m^3)

ACKNOWLEDGMENT

This work was supported by the National Science Council under Grant NSC 83-0402-E-007-002.

REFERENCES

1. R. T. Davis and S. A. Birdshell, "Hydrodynamic Model and Experiments for Crossflow Microfiltration," *Chem. Eng. Commun.*, *49*, 217 (1987).
2. R. Rautenbach and G. Schock, "Ultrafiltration of Macromolecular Solutions and Crossflow Microfiltration of Colloidal Suspensions. A Contribution to Permeate Flux Calculations," *J. Membr. Sci.*, *36*, 231 (1988).
3. C. A. Romero and R. H. Davis, "Experimental Verification of the Shear-Induced Hydrodynamic Diffusion Model of Crossflow Microfiltration," *Ibid.*, *62*, 249 (1991).
4. N. J. Blake, I. W. Cumming, and M. Streat, "Prediction of Steady Crossflow Filtration Using a Force Balance Model," *Ibid.*, *68*, 205 (1992).
5. V. L. Pillary and C. A. Buckley, "Cake Formation in Crossflow Microfiltration Systems," *Water Sci. Technol.*, *24*(10), 149 (1992).
6. G. Green and G. Belfort, "Fouling of Ultrafiltration Membrane: Lateral Migration and Particle Trajectory Model," *Desalination*, *35*, 129 (1980).
7. J. W. Hunt, C. J. Brouckaert, K. Treffry-Goatley, and C. A. Buckley, "The Unsteady-State Modeling of Crossflow Microfiltration," *Ibid.*, *64*, 443 (1987).
8. H. B. Dharmappa, J. Verink, R. Ben Aim, K. Yamamoto, and S. Vigneswaran, "A Comprehensive Model for Crossflow Filtration Incorporating Polydispersity of Influent," *J. Membr. Sci.*, *65*, 173 (1992).
9. W. M. Lu, K. J. Hwang, and S. C. Ju, "Studies on the Mechanism of Crossflow Filtration," *Chem. Eng. Sci.*, *48*, 863 (1993).
10. F. W. Altena and G. Belfort, "Lateral Migration of Spherical Particles in Porous Flow Channel: Application to Membrane Filtration," *Ibid.*, *39*, 343 (1984).
11. R. D. Cohen and R. F. Probstein, "Colloidal Fouling of Reverse Osmosis Membrane," *J. Colloid Interface Sci.*, *114*, 194 (1986).
12. M. R. Wiesner, M. M. Clark, and J. Mallevialle, "Membrane Filtration of Coagulated Suspensions," *J. Environ. Eng.*, *115*, 20 (1989).
13. M. Hartman, V. Havlin, O. Trnka, and M. Carsky, "Predicting the Free-Fall Velocities of Spheres," *Chem. Eng. Sci.*, *44*, 1743 (1989).
14. R. H. Davis, "Modeling of Fouling of Crossflow Microfiltration Membrane," *Sep. Purif. Methods*, *21*, 75 (1992).

15. M. R. Wiesner and S. Chellam, "Mass Transport Considerations for Pressure Driven Membrance Processes," *J. Am. Water Works Assoc.*, *84*, 88 (1992).
16. R. M. McDonogh, K. Welsch, A. G. Fane, and C. J. D. Fell, "Flux and Rejection in the Ultrafiltration of Colloids," *Desalination*, *70*, 251 (1988).
17. E. Iritani, T. Watanabe, and T. Murase, "Effect of pH and Solvent Density on Dead-End Upward Ultrafiltration," *J. Membr. Sci.*, *69*, 87 (1992).

Received by editor October 27, 1993